Surface Structure of a Complex Inorganic Crystal in Aqueous Solution from Classical Molecular Simulation

Michael Brunsteiner[†] and Sarah L. Price*

Department of Chemistry, University College London, 20 Gordon Street, London WC1H 0AJ, U.K.

Received: March 16, 2004; In Final Form: May 26, 2004

The theoretical investigation of polar crystal surfaces in solution involves methodological issues that have not been entirely resolved. Here we present results of molecular dynamics simulations of potash alum surfaces in contact with aqueous solution. As a prerequisite for this study, we developed a classical, empirical model potential for this complex inorganic material. The resulting rigid ion force field was carefully tested, and we could show its ability to reproduce a wide range of experimental results. Using this force field, we studied the (111) surface of potash alum and compared various ways of simulating this polar surface. By establishing the stability of a charged, in addition to the reconstructed crystal surface usually assumed, we question the common practice of excluding the existence of such charged surface terminations a priori.

1. Introduction

Knowledge of the detailed structures of crystal surfaces is important in a number of fields including catalysis,[1] crystal growth,[2] separation techniques,[3] semiconductors and industrially applied nanostructures.[4] Here we needed to establish the microscopic structure of potash alum (PA) crystal surfaces in aqueous solution to aid the interpretation of an experimental study on the agglomeration of PA crystals.[5] Neither experimental nor theoretical results for the detailed atomic scale structure of PA surfaces have been published so far. Here we apply theoretical methods based on molecular simulation to study PA in contact with aqueous solution and propose atomistic structures for its three major faces.

Modeling PA surfaces in contact with a solution is computationally not feasible at the electronic level. If we try to study the system via classical molecular simulation, we encounter a number of complications: It is comparatively complex, containing potassium and aluminum cations, sulfate anions showing dynamical disorder, and a substantial amount of water of crystallization. The surface dominating the morphology of PA crystals, the (111) face, cannot be assumed to be a simple cut through the bulk crystal, as this gives a polar face. Thus, studying the crystal−solution interfaces of PA requires the solution of a number of methodological problems in computational material surface science:

(i) Further consideration of how to model crystalline materials with a finite dipole moment in the unit cell perpendicular to a growing surface, so-called polar faces, is necessary. The most common approach for ionic materials is the reconstruction of the polar surfaces by a specific redestribution of ions between two opposing surfaces with Miller indices (hkl) and ($\bar{h}\bar{k}\bar{l}$).[6−9] As an alternative for this model, derived for crystals in a vacuum, we also consider a charged crystallite in a charge compenstating solution environment.

(ii) Classical molecular simulation of PA crystallites in solution requires parameters for modeling the solid, the liquid, and the interface. Force field parameters needed for the application of classical simulation of complex inorganic materials are limited in availability, and their transferability cannot be assumed. Thus we develop and validate a consistent force field for PA crystal and aqueous solution.

(iii) The relative stability of different crystal surfaces at a given temperature is determined by their surface free energies or surface tensions.[10] Methods for calculating surface free energies have been established[11−14] and applied to a small number of comparatively simple materials such as Lennard-Jones crystals,[13,15] pure metals,[14] or simple alloys.[16] With the hardware and algorithms currently available the calculation of surface free energies for more complex materials appears to be not feasible. An assumption commonly made is that the termination with the lowest surface energy (as opposed to surface *free* energy) is the most stable structure. Relative surface energies have been calculated with either empirical classical model potentials or diverse ab initio or DFT methods, and applications to inorganic materials include perovskite titanate,[17] forsterite,[18] aragonite,[19] and various metal oxides.[6,20,21]

Here we present details of a classical model potential we develop for potash alum and the results of calculations performed for its validation. We use this force field to model potash alum surfaces in contact with a saturated aqueous solution. By performing molecular dynamics simulations, we include the effect of the finite temperature and, thereby, implicitly, include entropic factors that cannot be observed with molecular mechanics and energy minimization. We find that we can assess the relative stability of different surface terminations at room temperature from the molecular dynamic simulations without needing to calculate the surface energy of a polar surface. Our results suggest that a polar surface does not necessarily have to be reconstructed to be stable. A combination of surface relaxation and the attachment of counterions and polar solvent molecules stabilizes a polar (effectively charged) surface as a viable alternative. The methodology that we develop here for PA surfaces in solution can also be applied to other systems.

* Corresponding author. E-mail: s.l.price@ucl.ac.uk.
[†] Current address: RDM Chemistry, Agfa-Gevaert N.V., Septestraat 27, B-2640 Mortsel, Belgium.

10.1021/jp0488259 CCC: $27.50
Published on Web 07/28/2004

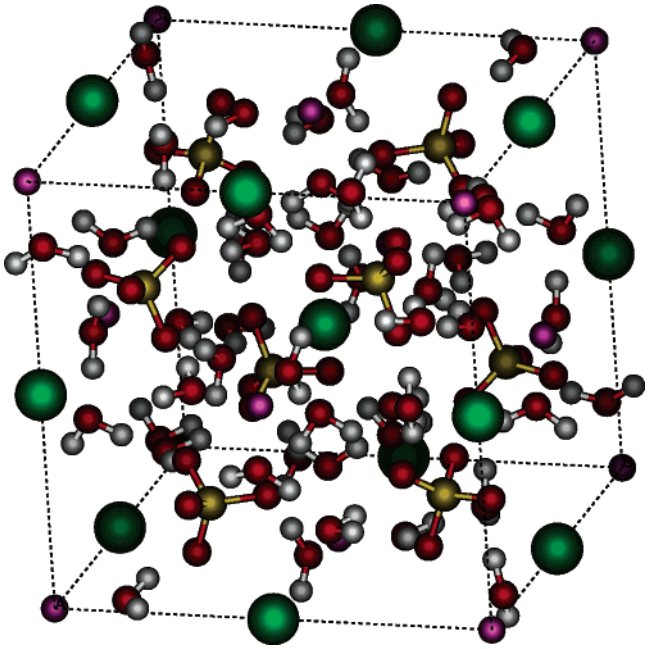

Figure 1. Ball and stick model of the structure of the potash alum unit cell. Atom types are identified by colors: green, K; magenta, Al; red, O; white, H; yellow, S.

2. Potash Alum and Possible Surfaces

2.1. Crystal. The cubic unit cell of potash alum (space-group $Pa\bar{3}$) contains four formula units $KAl(SO_4)_2 \cdot 12H_2O$ (see Figure 1) and was determined by X-ray diffraction.[22] To estimate the positions of the undetermined hydrogen atoms, we use the hydrogen positions determined by neutron diffraction[22] in the very similar $NH_4Al(SO_4)_2 \cdot 12H_2O$ unit cell, with the water molecule geometry defined by the SPC/E water model[23] that we use in our simulations.

A distinctive feature of potash alum is that the S−O bonds in each sulfate ion can be found either pointing toward the surrounding potassium ions (orientation B) or between them (A). This *dynamical disorder* varies with temperature and pressure. According to X-ray data between 70 and 90% of the sulfate groups are found in the energetically more favorable orientation A under ambient conditions.[24]

2.2. Surfaces. PA crystals in aqueous solution are usually terminated by large (111) and considerably smaller (200) and (220) faces.[25] Both the (111) and the (200) faces of PA have been shown to grow via a screw dislocation mechanism.[26,27] Therefore we can expect the surfaces to be flat over large regions from low up to intermediate supersaturations. For the (220) face, the high symmetry of the unit cell leaves us with only one possible cut to obtain a flat surface, as shown in Figure 2.

Although the (200) face would allow for at least three different cuts, only the one termination shown in Figure 2 results in a surface with a vanishing dipole moment perpendicular to that surface and so can be safely assumed to approximate the real surface structure.

A transverse section of the (111) surface as shown in Figure 2 demonstrates that each of the four possible simple cuts of the PA (111) face produces a polar surface as a consequence of the alternating staggering of positively (K^+ or Al^{3+}) and negatively charged (SO_4^{2-}) sublayers. These surfaces are all type III according to the categorization of ionic crystal surfaces (types I−III) introduced by Tasker[28] (Figure 3). This author argued that a polar or type III surface cannot exist on a real crystal because the dipole moment perpendicular to this surface, and therefore also the surface energy, diverge as the crystal grows. Tasker concluded that for all crystals with a theoretical type III surface this surface will reconstruct while growing, ending up as some version of a type II surface (rec-1 and rec-2 in Figure 3). For ionic materials reconstruction resulting in the elimination of the dipole moment is typically done by removing, e.g., half of the ions on one surface and relocating them on the opposite surface of a crystal slab. Thus a neutral sytem with with a zero dipole moment perpendicular to the surface is obtained and the surface energy can be calculated in the same way as it is done for nonpolar surfaces. However, if we are interested in the structure of these surfaces in contact with a polar liquid and/or ionic solution, we also have to consider alternative mechanisms that can reduce the dipole moment.

Modification of the electronic structure of the surfaces, as often proposed for polar oxide surfaces/semiconductors, will play a negligible role for strongly ionic crystals such as PA. Experimental microscopic data[26,27] show PA surfaces to be flat over regions of at least several nanometers. Therefore microfaceting as a mechanism of stabilization can also be excluded. Partially covalent bonding of hydroxy anions to surface aluminum ions could contribute to the stabilization of the surface. This process will be very sensitive to the pH of the solution and also could not be included in classical molecular simulation in a straightforward way. Hence we concentrate on the three mechanisms that can be expected to make the largest contribution to the stabilization of many polar ionic surfaces: surface relaxation, reconstruction, and the attachment of counterions or polar solvent molecules.

3. Methodology and Computational Details

All MD simulations are performed with a modified version of DL_POLY.[29] Electrostatic long-range interactions are calculated with a smooth particle mesh Ewald algorithm.[30] For the simulations of surface geometries this 3D-Ewald algorithm was complemented by a correction term minimizing interactions between adjectant crystal slabs.[31] The van der Waals interactions are cut off at a distance of 12 Å. Where appropriate, correction terms for the energy and forces calculated for systems with a permanent dipole moment[31] and the for energy of systems with a net charge[32] are applied. The temperature is kept constant at 300 K with a Nose-Hoover thermostat.[33] A SHAKE-like algorithm[34] is used to keep the water molecules rigid. For the calculation of the crystal structure at zero K and elastic constants, we use the program GULP.[35]

3.1. Classical Model Potential. The water water interactions are modeled by the widely used SPC/E rigid water model, which provides good results for many properties of liquid water.[23] The SPC/E partial charges result in a considerably higher dipole moment than the isolated water molecule, which, at least partially, makes up for the omission of polarization terms. The intramolecular parameters for SO_4^{2-} anion, described by a Morse (bond stretching, eq 1) and harmonic bond bending potential (eq 2) were fitted by Allen et al.[36] to reproduce crystal structures of a range of different sulfates of mono- and divalent cations. Formal charges were used for Al^{3+} and K^+ cations. The sulfate oxygens (OS) were assumed to interact which each other and with the water oxygens (OW) by a Lennard-Jones potential (eq 3) for consistency with the SPC/E water potential. For the K^+−water van der Waals interactions we used a potential parametrized by Borodin et al.[37] who fitted Buckingham potential parameters to reproduce structures of a range of different K^+−SPC/E water clusters minimized at the MP2 level with large basis sets. Additional repulsion−dispersion potentials

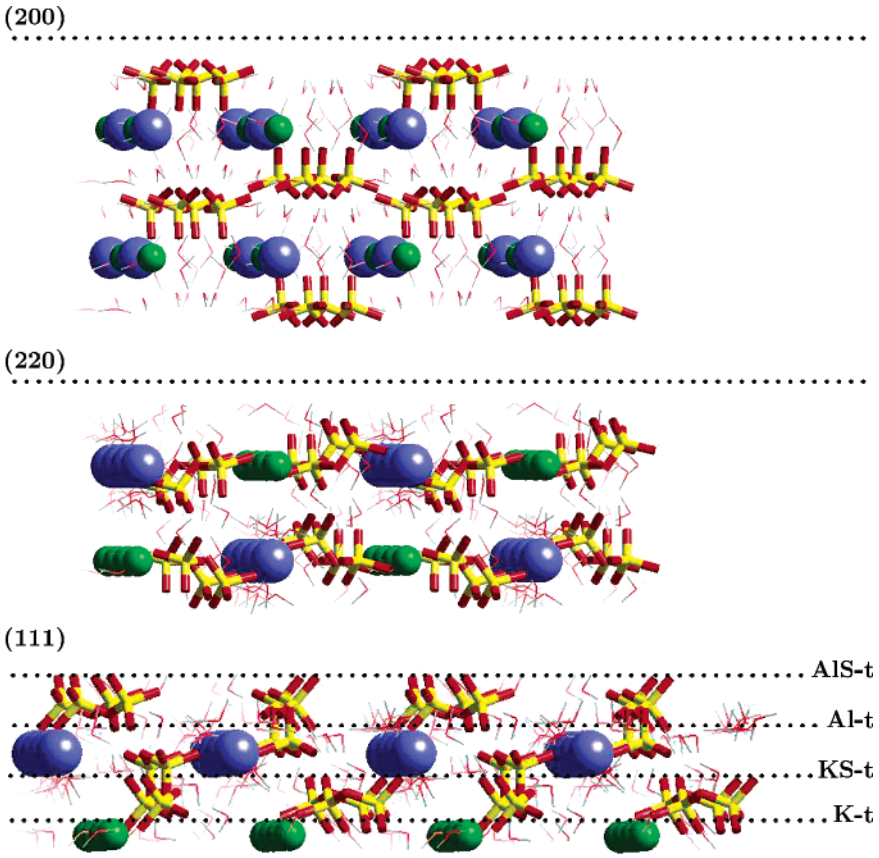

Figure 2. Atomic structure of the potash alum surfaces. Each slab contains four PA unit cells. Shown are cross sections of the crystal with the surfaces on top. The surface terminations considered here are indicated by dotted lines.

(which were assumed to be in the more accurate form of eq 4) and sulfate partial charges have to be compatible with the above parameters. These remaining parameters were fitted to reproduce the crystal structures of PA, K_2SO_4, $Al_2(SO_4)_3$, and $KAl(SO_4)_2$, the elastic constant matrix of PA, and the structures of the two hexaquo complexes, $[Al(H_2O)_6]^{3+}$ and $[SO_4(H_2O)_6]^{2-}$.

$$U_{\text{bond}}(b) = D\{[1 - \exp(-\beta(b - b_0))]^2 - 1\} \quad (1)$$

$$U_{\text{ang}}(\alpha) = \frac{1}{2}k_a(\alpha - \alpha_0)^2 \quad (2)$$

$$U_{\text{LJ}}(r_{ij}) = 4\epsilon\left\{\left(\frac{\sigma_{ij}}{r_{ij}}\right)^{12} - \left(\frac{\sigma_{ij}}{r_{ij}}\right)^{6}\right\} \quad (3)$$

$$U_{\text{Buck}}(r_{ij}) = A_{ij}\exp(-r_{ij}/\rho_{ij}) - C_{ij}r_{ij}^{-6} \quad (4)$$

We want to stress that the resulting model potential must be considered as a purely empirical force field, developed using more realistic functional forms for the additional intermolecular interactions, but having the benefit of established parametrizations. The parameter set is tested by performing molecular dynamics simulations of the bulk crystal and aqueous solutions of the various ions at a temperature of 300 K and a pressure of zero bar using DL_POLY.[29] The final parameter set, henceforth referred to as PAFF, is given in Table 1.

3.2. Validation of the Model Potential. In Table 2 the results of the lattice energy minimizations for three different anhydrate compounds using the PAFF parameters are given. Although no space group constraints were applied the symmetry was conserved in all cases. The results for K_2SO_4 and $Al_2(SO_4)_3$ are reasonable with the largest deviation from cell parameters or cell volume being 2.64%. The cause of the relatively large error of 8.74% for the cell volume of $KAl_2(SO_4)_2$ is probably the high charge of the aluminum cation in combination with the use of nonpolarizable sulfate anions. This is irrelevant for modeling the PA crystal in solution as the highly charged Al^{3+} cation is always shielded by a water layer. The experimental rate constant for the exchange of water molecules in the $[Al(OH_2)_6]^{3+}$ complex is 1.29 s^{-1}[38] and, as shown below, the proposed force field provides a good reprentation of the $[Al(OH_2)_6]^{3+}$ complex.

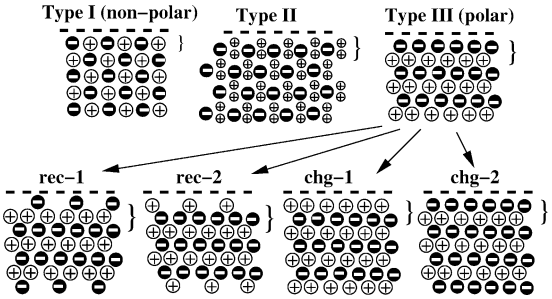

Figure 3. Schematic illustration of the different types of surface terminations. Crystal slabs are shown in side view, the dashed line indicating the position of the surface. The repeat unit is indicated by the curly brackets. Both types II and III surfaces have layers with alternating net charges perpendicular to the surface, but in type II faces the stoichiometric repeat unit can be defined so that a zero net dipole moment results. The dipole moment of the polar surface can be eliminated by *reconstructing* (rec) the crystal slab, resulting effectively in a type II surface, or by *charging* it (chg).

Lattice parameters and cell volumes after lattice energy minimization of PA compare well with experimental values (Table 3), and the symmetry is conserved. The elastic constants as obtained with PAFF are considerably higher than experi-

TABLE 1: Parameters for a Potash Alum Force Field (Units: eV, Å, and e)

atom types	pot. type			
O_W-O_W	Lennard-Jones	$\epsilon = 6.727e-03$	$\sigma = 3.166$	
O_W-O_S	Lennard-Jones	$\epsilon = 6.727e-03$	$\sigma = 3.166$	
O_S-O_S	Lennard-Jones	$\epsilon = 1.411e-02$	$\sigma = 2.798$	
$Al-O_S$	Buckingham	$A = 1000.0$	$\rho = 0.2670$	$C = 0.0$
$Al-O_W$	Buckingham	$A = 1000.0$	$\rho = 0.2670$	$C = 0.0$
$K-O_S$	Buckingham	$A = 2121.0$	$\rho = 0.2924$	$C = 2842.2$
$K-O_W$	Buckingham	$A = 2121.0$	$\rho = 0.2924$	$C = 2842.2$
O_S-S-O_S	harmonic	$k_b = 15.0$	$\alpha_0 = 109.47°$	
$S-O_S$	Morse	$D = 5.0$	$\beta = 1.2$	$b_0 = 1.505$

atomic charges

$q(O_W) = -0.8476$	$q(H) = 0.4238$	$q(S) = 2.2$
$q(O_S) = -1.05$	$q(Al) = 3.0$	$q(K) = 1.0$

TABLE 2: Results of Lattice Energy Minimizations of the Crystalline Anhydrates[a]

	K_2SO_4[41]		$Al_2(SO_4)_3$[42]		$KAl_2(SO_4)_2$[43]	
	exptl	PAFF	exptl	PAFF	exptl	PAFF
a/Å	5.723	+2.14	8.025	+1.34	4.71	+4.26
b/Å	9.999	−0.69	8.025	+1.34	4.71	+4.26
c/Å	7.422	−1.95	21.357	−2.64	8.01	+0.03
V/Å^3	424.7	−0.54	1191.1	−0.01	153.9	+8.74

[a] For each material the experimental (exptl) lattice parameters and unit cell volume are given, with the % deviations obtained with the PAFF force field.

TABLE 3: Results of Lattice Energy Minimizations of Potash Alum, Compared to Experimental Results

lattice params	exptl[22]	PAFF	Δ/%	elastic constants/ 10^{11} Dyn/cm^2	exptl[44]	PAFF	Δ/%
a/Å	12.157	12.096	−0.50	e_{11}	2.47	4.88	+98
b/Å	12.157	12.096	−0.50	e_{12}	1.03	1.61	+56
c/Å	12.157	12.096	−0.50	e_{44}	0.87	1.01	+16
V/Å^3	1796.7	1769.8	−1.50				
Average Distance between Selected Atom Types/Å							
O1−S	1.4830	1.4601	−1.544	O2−Al	1.9077	1.8968	−0.571
O1−O1	2.4213	2.3840	−1.540	O2−O1	2.6830	2.5999	−3.097
O2−K	2.9825	2.9926	+0.339	O2−O2	2.6666	2.6646	−0.075

mental values but calculated elastic constants are generally expected to be larger than those obtained in experiment because in real crystals we usually find defects such as vacancies, grain boundaries, etc. whereas the theoretical model corresponds to a perfect crystal at zero K. Here we consider it sufficient to get elastic constants that are qualitatively correct but larger than the experimental values.

The aluminum−oxygen distance in the $[Al(H_2O)_6]^{3+}$ cluster after energy minimization is 1.946 Å, comparing well with high-level ab initio calculations of this complex (1.953 Å).[38] The distance between sulfate and water oxygens in the $[SO_4(H_2O)_6]^{2-}$ cluster as obtained after energy minimization is 2.75 Å, which is smaller than the experimental value of 2.88 Å obtained for the complex in solution at 298 K. The difference between the two distances can, at least in part, be attributed to the thermal motion.

In the molecular dynamics simulation of the PA crystal at ambient conditions the symmetry and the structure are well conserved. The average lattice parameter is only 0.2% larger than the experimental value.[22] As shown by the calculated radial distribution functions in Figure 4, the first maxima of the pair correlation functions coincide generally quite well with the experimental distances from X-ray data, shown as δ functions. The small deviations in distribution functions including sulfate oxygens are mainly due to the orientational disorder of the sulfate groups.

TABLE 4: Radii of Solvation Shells ($\langle\,\rangle$, Å) and Diffusion Coefficients (D, 10^{-9}m^2/s) Obtained in MD Simulations of Solutions of Eight K_2SO_4 in 436 H_2O or Eight $Al_2(SO_4)_3$ in 800 H_2O, Respectively, at 300 K[a]

K_2SO_4	MD	exptl	ref	$Al_2(SO_4)_3$	MD	exptl	ref
$\langle K-O_W\rangle$	2.74	2.79	45	$\langle Al-O_W\rangle$	1.91	1.90	46
$\langle O_S-O_W\rangle$	2.68	2.79	47	D (Al^{3+})	0.82		
$\langle S-O_W\rangle$/	3.71	3.7−3.9	48				
coord no. (K^+)	6.7	6−7	45				
coord no. (SO_4^{2-})	12.8	6−14	48				
D (K^+)	1.4	2.0	49				

[a] The average radius of the first solvation shell for the different ionic species is taken to be the distance of the first maximum of the corresponding radial distribution function from the origin.

For quantifying the degree of disorder we define the order parameter

$$O_{PA} = \frac{N_A}{N_A + N_B} \tag{5}$$

N_A and N_B being the numbers of sulfate atoms in orientation A or B, respectively (cf. section 2.1). The numbers are obtained by monitoring the angle between the lines from each potassium ion to its neighboring sulfate atoms and the bond between each sulfate atom and the oxygen closest to the potassium ion. Molecular dynamics simulation at 300 K and zero pressure gives a degree of disorder of $O_{PA} \approx 0.95$. This is acceptably larger than the experimental value of 70−90% considering the high uncertainty of the experimental value. We also performed a simulation run of a PA crystal at a pressure of one GPa. Starting from the experimental crystal structure with $O_{PA} = 1.0$, there is complete disorder; i.e., on average, half of the sulfate ions are to be found in either orientation, after a simulation time of about 40 ps. Though there is no order in the sulfate orientations, the metal atoms are still ordered and remain close to their ideal lattice positions. This intriguing result of decreasing order in a crystal with increasing pressure has been confirmed experimentally[24] for potash alum and can be seen as a further confirmation of the predictive power of our force field.

Table 4 shows that molecular dynamics simulations of K_2SO_4 and $Al_2(SO_4)_3$ solutions at ambient conditions yield solvation shell radii and a K^+ diffusion coefficient in good agreement with experimental values. The agreement of the diffusion coefficient with experiment may be fortuitous given our relatively short simulation times.

The $Al^{3+}-O(SO_4^{2-})$ distribution function (not shown) reveals the occurrence of occasional contact ion pairs with an $Al^{3+}-O(SO_4^{2-})$ distance of only 1.6 Å. This is encouraging because contact ion pairs between aluminum and anions in aqueous solutions are generally not found with other anions such as ClO_4^-, Cl^-, or NO_3^- but are confirmed experimentally for SO_4^{2-}.[38]

3.3. Molecular Dynamics Simulations of the Interfaces. Molecular dynamics simulations are performed of a saturated PA solution adjacent to PA crystal slabs with different surface terminations exposed to the solution. The crystal slabs consist of layers of 2 × 2 surface unit cells, the number of layers varying between 3.0 and 3.75 for different terminations as detailed below. The simulation cell geometry used in all cases is shown in Figure 5. The crystal slab is placed on one end of the box with the surface of interest perpendicular to the z direction and facing the solution layer. At least the uppermost

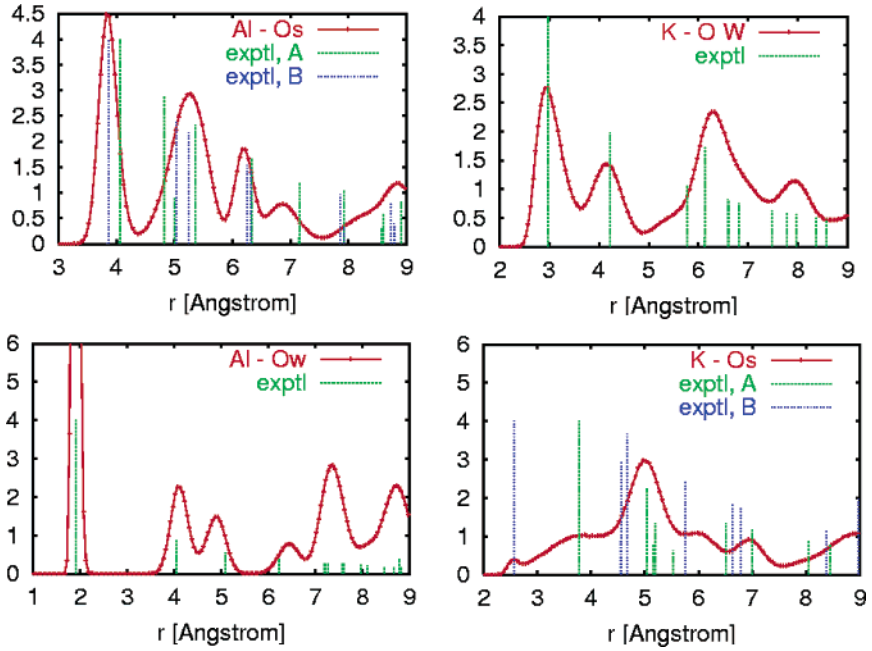

Figure 4. Radial distribution functions obtained for various pairs of atom types in a 200 ps molecular dynamics simulation of a potash alum 2 × 2 × 2 supercell at 300 K and a pressure of 0 Pa. The average structure at this temperature as obtained with X-ray diffraction is indicated by δ functions.

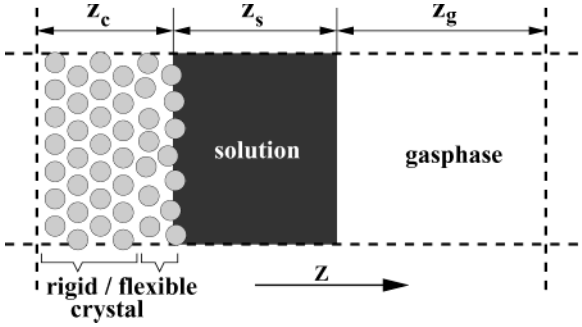

Figure 5. Cross section of the MD simulation cell. Each system consists of a PA crystal slab with one of the considered surface terminations in the *xy* plane, adjacent to a layer of saturated PA solution. Only the atoms in the sublayers of the crystal slab close to the solution are allowed to move (flexible); the remaining atoms of the crystal are frozen (rigid). Periodic boundary conditions are imposed in all dimensions; a void region is introduced to approximate an effectively two-dimensional system. The dimensions of the cell parallel to the interface are 34.38 × 29.78 Å (111 surface), 24.31 × 24.31 (200 surface), and 34.38 × 24.31 Å (220 surface).

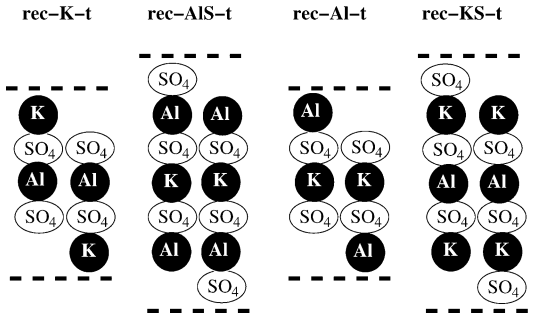

Figure 6. Possible reconstructions (type III ⟹ type II) of the polar potash alum (111) face. The position of the two surfaces of each slab are indicated by the dashed bold lines. The many bulk unit cells that would separate the two faces have been omitted for clarity. Note that there are three sulfate ions per surface unit cell in the terminating sulfate layer for AlS-t, and only one for KS-t, due to the different charges in the adjacent Al^{3+} and K^+ layers, respectively, though this is not apparent from this view.

three sublayers of sulfate ions and cations in the crystal slab, including the corresponding crystal water molecules, are allowed to move freely according to the intermolecular forces due to all the other molecules in the system whereas the remaining part of the crystal is held rigid in the course of the simulation.

The length of the box in the *z* dimension is in all cases 70 Å. In all simulations the solution consists of six sulfate, three aluminum, and three potassium ions in 576 water molecules, corresponding to a PA solution at the saturation concentration at 300 K of 121.2 g of anhydrous PA per 1 kg solution. With the resulting thickness of the solution layer, z_s, between 15 and 20 Å, this leaves a vacuum slab of $z_v \approx 25$ Å. In the simulations, there were generally zero, or one or two, water molecules in the vacuum layer, so the ionic concentration in the solution layer remained effectvely constant over the whole simulation time.

The slab terminations considered are the two nonpolar surfaces (labeled 200-t and 220-t) and eight different (111) surfaces. Four of the latter are reconstructed as sketched and labeled in Figure 6. Each one of four nonreconstructed (111) slabs is set up in two different ways: (1) the *charged version* (see chg-1 or chg-2 in Figure 3) and (2) the *polar version*, corresponding essentially to three layers of the slab shown in Figure 2 (see *polar* in Figure 3).

The structure of the surface exposed to the solution is identical for both the charged and the polar version. They differ only by one additional rigid sublayer at the bottom, leaving the charged version with its net charge but with a zero dipole moment. If one uses the 3-D Ewald summation technique to account for the electrostatic long-range interaction in a simulation, any net charge is implicitly compensated for by the introduction of a homogeneously distributed background charge of the same magnitude and the opposite sign. Such a homogeneous background charge density can be seen as a simple approximation of the effect of the diffuse and nonhomogeneous counterion cloud to be found above real charged surfaces in aqueous solutions.[39] Although this is a rather crude model, we prefer this setup compared to the introduction of an abitrary amount of explicit counterions. Because we cannot know the width of

TABLE 5: Details of the Molecular Dynamics Simulations

label	surf[a]	occ[b]	N_l[c]	label	surf	occ	N_l
chg-AlS-t	SO_4^{2-}	1.0	3.75	chg-Al-t	Al^{3+}	1.0	3.25
rec-AlS-t	SO_4^{2-}	0.75	3.625	rec-Al-t	Al^{3+}	0.5	3.0
pol-AlS-t	SO_4^{2-}	1.0	3.0	pol-Al-t	Al^{3+}	1.0	3.0
chg-KS-t	SO_4^{2-}	1.0	3.75	chg-K−t	K^+	1.0	3.25
rec-KS-t	SO_4^{2-}	0.25	3.375	rec-K−t	K^+	0.5	3.0
pol-KS-t	SO_4^{2-}	1.0	3.0	pol-K−t	K^+	1.0	3.0
200-t	SO_4^{2-}	1.0	3.0	220-t	all	1.0	3.0

[a] Type of ions in the outermost surface layer. [b] Occupancy of the outermost surface layer, 1 for a full layer as in the bulk, 0.5 for a half layer, etc. [c] Number of layers of surface unit cells in the slab: each layer consists of four sublayers, each sublayer contains 16 ions of only one type, all ions are equally weighted.

the counterion layer a priori and cannot currently model a system size large enough for this to be determined by simulation, the use of counterions could easily lead to other artifacts.

According to the label assigned to each surface in Figure 2 and to whether the charged or polar version was used, the simulation runs are labeled chg-AlS-t, pol-AlS-t, chg-Al-t, etc. The reason for setting up simulations with the polar in addition to the charged slabs is that it is unclear a priori which of the two setups gives the more faithful representation of the system. Comparing the results allows us to estimate the nature and magnitude of any artifacts that are possibly introduced by either method.

All systems are equilibrated for at least 50 ps with the entire crystal slab held rigid. After this equilibration period, the atoms in the uppermost sublayers of the crystal slab are allowed to move freely. The overall simulation time for each of the different systems is at least 200 ps. The most stable terminations are simulated for considerably longer time spans specified in the results section. More details on the geometries and other features of the different simulations are given in Table 5.

4. Results of Simulations of the Potash Alum Solution Interfaces

4.1. Nonpolar Surfaces. The structures of the two systems with the nonpolar PA surfaces are shown in Figure 7 where snapshots of the simulation cells at the end of each simulation and density profiles for the ions along the direction perpendicular to the surface are shown. The flexible surface ion layers are relatively stable. The dissolution of one single ion, corresponding to a small peak at approximately $z = 0$ Å in the density distribution, can be seen above the (200) surface. The rest of this surface, however, remains stable over the whole simulation time of 600 ps. The peaks between $z = -5$ and -20 Å in the density distribution plots corresponding to the flexible Al^{3+}, K^+, and sulfate layer, become broader as the interface is approached (increasing z). However, even the width of the broadest peak, corresponding to the uppermost sulfate layer at $z \approx -6$ Å, would not exceed ~2 Å, which can be considered as appropriate for surface atoms in a stable interface at a temperature of 300 K.

In the ~25 Å thick solution of PA above the surface, barely any ordering of Al^{3+} occurs. The reason for this is probably that Al^{3+} ions are always surrounded by a very tight and persistent hydration shell of six water molecules. The exchange rate of the waters in the K^+ hydration shell is faster by about 8 orders of magnitude.[38,40] The water molecules closest to the surface are also very tightly bound and hardly any exchange of these waters happens in the course of the simulation. Therefore there will always be at least two relatively rigid layers of water between any aluminum ion and the surface. The potassium ions never attach directly to the (200) surface; i.e., there is always at least one water molecule between the solution potassium ions and each surface sulfate oxygen atom.

In the snapshot of the (220) surface in Figure 7, two of the K^+ ions are about 2 Å from their ideal lattice positions but there was no sign of a real dissolution of the surface. Within a simulation time of 600 ps the two K^+ ions diffused even further away from the surface as to be seen by the small peaks between $z = -2$ and -3 Å in the density distribution plots on the right-hand side but eventually they returned to a position nearer to their ideal lattice positions. Just as in the (200) surface the remaining ions in the surface remain stable. The solution above the (220) surface shows a more ordered structure than it does above the (200) surface, with a more pronounced trend for the potassium ions to get closer to the surface than Al^{3+} and sulfate ions.

4.2. (111) Surface. In all the simulations that were equilibrated with a potassium surface layer on the (111) face (K-t and KS-t), these surfaces are unstable. More than half the ions in the outermost surface layer of all the reconstructed, the charged and the polar K-t and KS-t terminations show a clear tendency to dissolve into the solution after less than 100 ps of simulation. Therefore only simulations of the hydrated aluminum ions surfaces, the AlS-t and Al-t terminations, could be extended to obtain convergence of the distribution functions of the ions in the solution above the surface.

The diagrams in Figure 8 demonstrate the stability of the reconstructed aluminum sulfate rec-AlS-t surface where the width of the distribution functions for the atoms are smaller than 1.5 Å and remain so over a period of 800 ps. Although the rec-AlS-t slab is overall neutral, it represents a type II face having charged sublayers. It is probably the resulting local electrostatic field that causes the structuring of the solution which is more pronounced here than it is above the nonpolar (200) and (220) faces. Again, a potassium peak at about $z = 0$ Å is next to the surface followed by aluminum and sulfate peaks at roughly identical positions. Going further out, the solution becomes increasingly disordered. The most notable observation here is that the potassium ions come in direct contact with the surface sulfate ions with no interstitial water molecules.

The reconstructed aluminum surface (rec-Al-t system, Figure 8) shows a somewhat broader outermost aluminum peak, but it still can be regarded as a stable surface termination. Due to the highly charged aluminum ions being directly on the surface, the local electrostatic field is stronger than it is in the rec-AlS-t system, and therefore the structure of the solution ions is even more distinctive here. Despite the positive charge of the outermost crystal layer the potassium ions get still closer to the surface than the sulfates. Potassium ions diffuse into the empty aluminum pockets left by the reconstruction (see Figure 8). One K^+ ion from the solution diffuses to the surface site after ~200 ps and stays in this position for 600 ps before diffusing back into the solution. A second attaches after 600 ps and stays there for 400 ps until the end of the simulation. This behavior is probably induced by the assumed artificial reconstruction of the surface. "In vivo" such a persistent attachment of K^+ ions in Al-sites is a very unlikely scenario because this one component of PA (the potassium ions) would act as an inhibitor for the growth of PA because the potassium ions got stuck in a "wrong" position on the surface. The structures of the two net-charged crystal slabs and the adjacent solutions (chg-AlS and chg-Al) are shown in Figure 9. The flexible surface layers in the chg-AlS system, one aluminum and three sulfate sublayers, are stable and have the lowest amplitude of vibrations normal to the

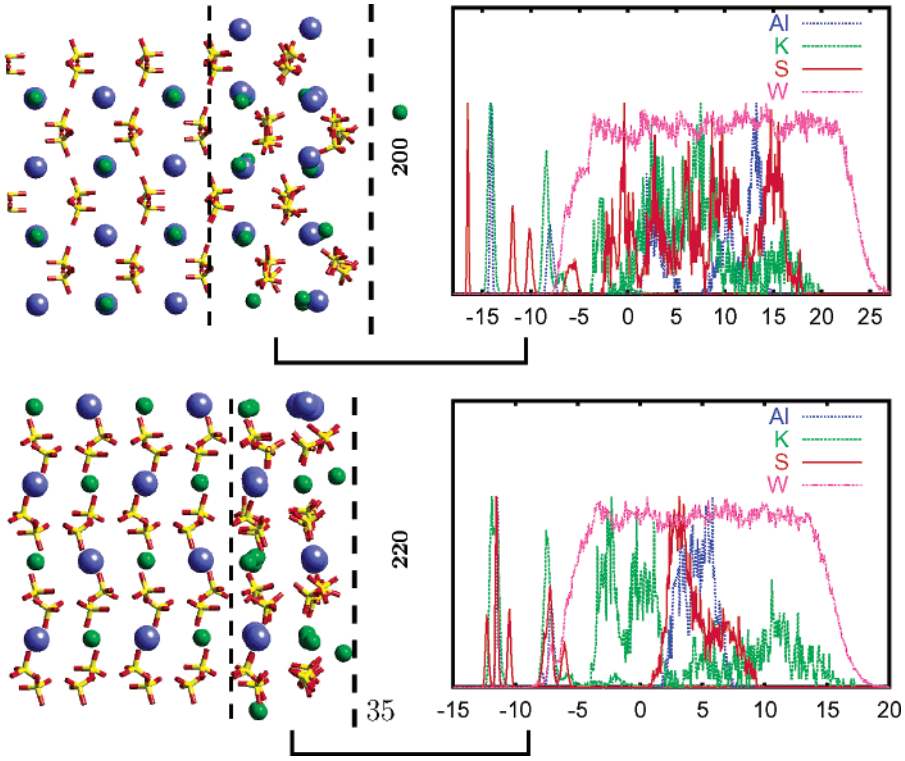

Figure 7. Structure of the (200) and (220) surfaces and the solution, snapshots and *z* density distribution functions. The thick dashed line marks the surface, and the thin dashed line marks the boundary between rigid and flexible ions. The abscissa in the distribution function plots corresponds to the *z* dimension in Figure 5 with units of Å. For easier comparison the peaks in the density distribution function plots have been normalized so that their maxima are approximately at equal heights and a horizontal brace connects a layer in the snapshot with the corresponding peak in the distribution function plot. The crystal water is included neither in the snapshots nor in the distribution function plots for clarity. The water considered here includes only water present in the solution in the initial configuration, which is valid because very few of the crystal waters diffused into the solution.

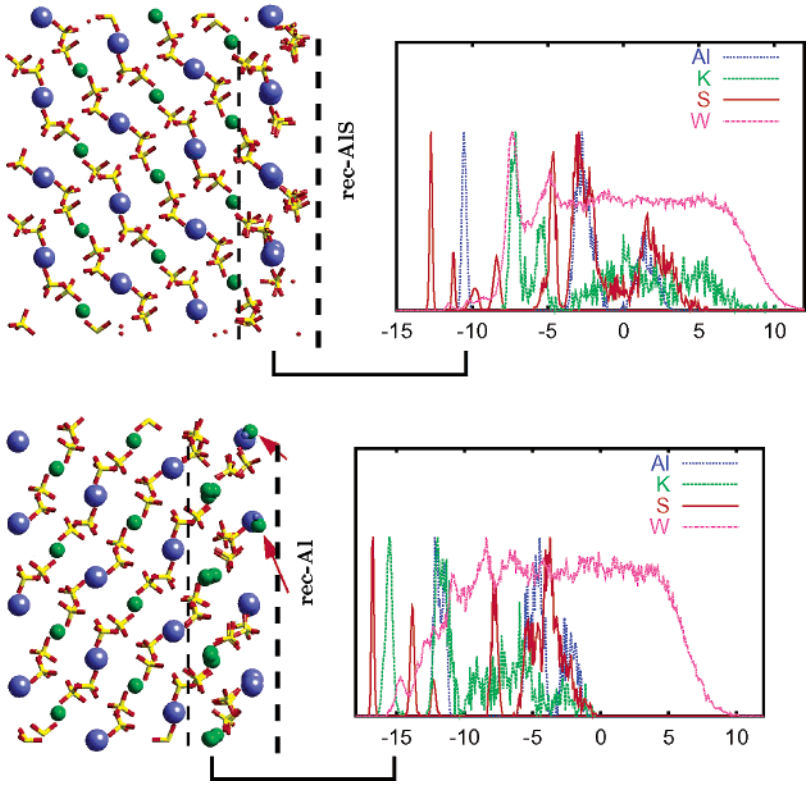

Figure 8. Structure of the reconstructed (111) surface and the solution. The arrows in the snapshot of the rec-Al-t system show the K^+ ions that have attached to the surface from the solution. Adjacent Al^{3+} ions are drawn smaller for clarity. See the caption of Figure 7 for more details.

surface of any of the model (111) surfaces. The solution above the surface including the water is well ordered.

The other charged surface model, chg-Al, gives a quite stable surface (Figure 9) but a uniquely clear ordering of the ions in

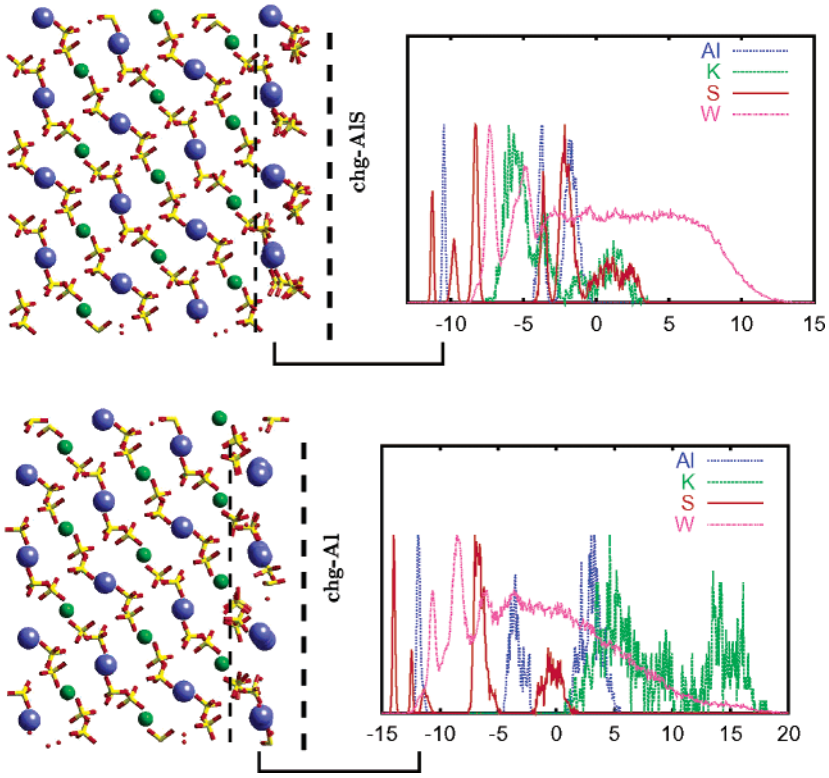

Figure 9. Structure of the charged (111) surfaces and solutions. See the caption of Figure 7 for more explanations.

the solution perpendicular to the surface. There are two water layers closest to the surface, followed by a succession of four distinctive sulfate and aluminum peaks (surface$-Al^{3+}-H_2O-H_2O-SO_4^{2-}-Al^{3+}-SO_4^{2-}-Al^{3+}$). Potassium ions, with a couple of hydration waters appear to evaporate into the gas phase. We note that the magnitude of the net-charge of the PA slab in the chg-Al system (32 e per simulation box) is twice as large than it is in the chg-AlS system. Thus this high charge density probably causes the ionic layering in the solution and the resulting oscillating charge density. The very ragged gas liquid interface is clearly an artifact due to the small system size. It is somewhat surprising that, despite the high charge density in the slab, the structure of the flexible surface layers is barely distorted and the atoms in the surface remain very close to their ideal lattice positions.

To make sure that no artifacts were introduced by holding the majority of the crystal ions rigid in the simulation, the chg-AlS-t system was simulated for 400 ps with one additional layer of each K^+ and Al^{3+} and the according number of sulfate and water molecules flexible. The width of *z* distribution functions of the outermost surface ions increases slightly, but the surface remains stable and no dissolution of ions into the solution is observed, hence confirming the qualitative behavior of the chg-AlS-t surface shown in Figure 9.

The results obtained with the polar slabs with either two (pol-Al) or three (pol-AlS) sulfate layers, one aluminum layer and the corresponding waters of crystallization are shown in Figure 10. Both surfaces remain flat and stable over the simulation period of 200 ps for pol-Al and two ns for pol-AlS. However, the structure of both surfaces differs considerably from the bulk crystal structure. In the pol-AlS surface the distance between the surface aluminum layer and the first rigid aluminum layer in the bulk increases markedly in comparison to the ideal crystal structure. In the pol-AlS density distribution plot, the position of the aluminum peak with respect to the three sulfate peaks is shifted toward the surface. In the pol-Al surface the sulfate peaks also move outward with respect to the aluminum layers. In both cases this pronounced relaxation leads to a decrease in the net *z* dipole moment. The peaks in the *z* distribution of the surface ions are broader than in the charged or reconstructed versions. The net dipole moment in the un-relaxed pol-Al slab is larger than it is in the pol-AlS system, which accounts for the relaxation as well as disorder being more pronounced in the pol-Al than in the pol-AlS surface.

5. Discussion

5.1. Structure of the PA (111) Surface. In our simulations, the PA solution above the surfaces is saturated. For a real system this corresponds to a steady state with the crystal dissolving and growing at the same velocity. PA grows layer-wise via a screw dislocation mechanism[26,27] with growth and dissolution happening at step and kink sites on the crystal surface at low supersaturations. Thus, in our simulations we expect to find a stable surface cut that represents the termination found on growing PA (111) layers with other possible terminations dissolving. Applying this criterion, we can exclude all the potassium terminated surfaces (KS-t and K-t) which dissolve in the simulation. Both the reconstructed, the charged and the polar AlS-t and Al-t terminations are relatively stable. A strong point against the reconstructed Al-t surface is the fact that potassium ions block the empty aluminum sites produced by the reconstruction thereby thwarting further crystal growth.

The amplitude of the motions within the surface, as opposed to actual dissolution, is not necessarily a measure of the stability of the surface. In both the charged and the reconstructed systems the amplitudes of the vibrations of ions perpendicular to the surface are larger with the Al-t as compared to AlS-t termination. However, for the charged surface, this may just result from the charge density on the chg-AlS-t surface being half that on the chg-Al-t surface. The resulting strong electrostatic field above the surface causes a far-reaching ordering of ion layers in the

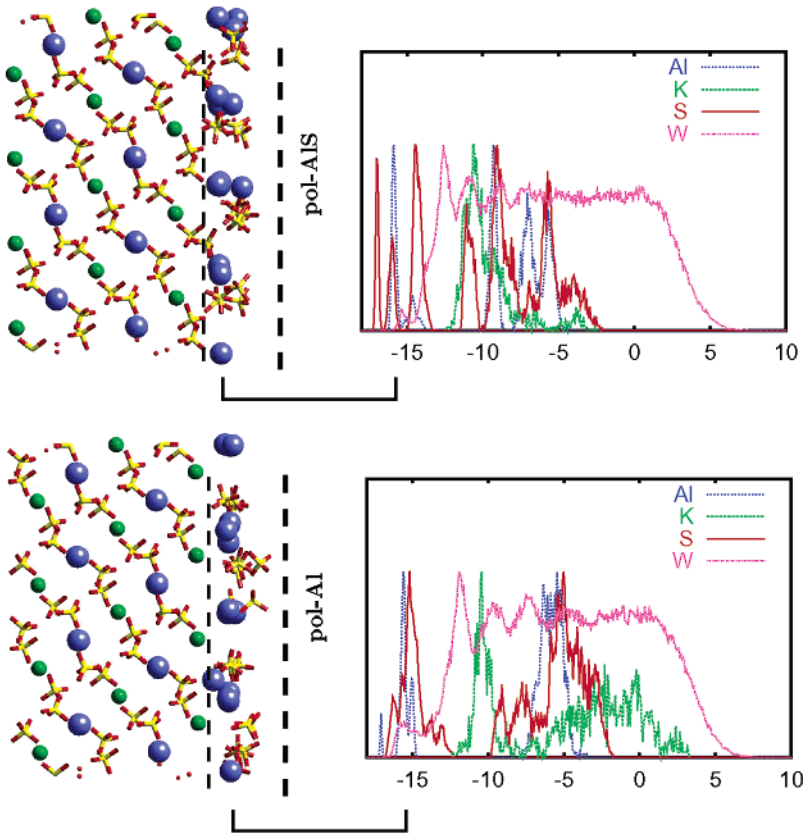

Figure 10. Structure of the polar (111) surfaces and solutions. See the caption of Figure 7 for more explanations.

solution, which will reduce the entropy of the system and thereby to increase the free energy making the occurrence of this type of surface termination generally less likely.

The theoretical results presented here suggest that the real PA (111) surface is terminated by an aluminum−sulfate layer (AlS-t). It is not possible at this point to determine clearly whether a reconstructed termination with only a fraction of the sites in the outermost sulfate layer occupied (rec-AlS-t) or a charged termination with a full sulfate layer on top of the surface (chg-AlS-t) is more likely to occur on a real crystal in aqueous solution. However, because the stability of both terminations seems to be quite similar, we expect combinations of both terminations to be found on real surfaces with the actual sulfate coverage depending on the activity of the sulfate ions in the solution.

It has been shown experimentally[5] that a pair of two (200) or two (220) faces form a stronger agglomerative bond than a pair of (111) faces. This must be a consequence of the structures of the surfaces involved and the atomistic models of the surfaces produced by our simulations can explain this phenomenon: If two (200) or two (220) faces attach, a crystalline bridge can be formed without any further rearrangement of ions or molecules because just by lateral movement two attached (220) or (200) surfaces can build a perfect crystal structure (see Figure 2). In contrast, whatever way we bring two (111) faces together, they cannot directly attach to form a perfect crystalline bridge. First, the polar surfaces are more relaxed than the nonpolar surfaces and this relaxation must be reversed. Second, additional ions from the solution are needed to build a stoichiometrically perfect crystal bridge. With the termination proposed here, a mixture between rec-AlS-t and chg-AlS-t, additional sulfate and potassium ions have to be brought in position before a continuous PA crystal can be formed. This requires time and energy, and therefore the strength of a crystalline bridge between two (111) faces will be weaker than that between two (200) or (220) faces for similar growth times.

5.2. Comparison of Different Computational Models for Polar Surfaces. We have simulated all four un-reconstructed surface terminations in a polar and a charged version. The results of the two simulations cannot be compared directly because the dipole correction term, only used in the simulations of the polar systems, affects not only the energy but also the forces on the atoms and thereby the structure of the flexible part of the crystal and the solution. However, the same surface terminations turned out to be stable with both methods and in agreement with the stability of the reconstructed model surfaces. This suggests that, at least for the material studied here, the methodology used to model the polar surface is not crucial for determining the stability of a given termination. Nevertheless, the likelihood of simulation artifacts, and of real crystal surfaces not corresponding precisely to any of these models, suggests that a range of simulation models should be considered for computational studies of other polar ionic surfaces in solution.

We consider the charged model of the polar surface as a more realistic representation of the system because it is more likely to occur in nature than the polar version, as modeled here. The homogeneous charge background used in the charged sytem is obviously a crude approximation to the nonhomogeneous charge distribution to be found above real polar surfaces. In the future this approximation could be evaluated by comparing the resulting liquid structure to a charge-neutral system with an appropriate surplus of counterions in the solution. In contrast to the dipole correction term, the homogeneous background charge can be seen as first-order approximation that is capable of systematic improvement.

6. Conclusions

We have developed a classical rigid ion model potential for potash alum and its aqueous solution. We could show that such a force field, if carefully optimized, can reproduce a wide range of properties of this rather complex inorganic material. Using this force field we performed molecular dynamics simulations of potash alum surfaces in contact with a saturated aqueous solution. Our results suggest that the potash alum (111) surfaces are terminated by a full aluminum sublayer and an outermost sulfate layer with a coverage probably depending on the sulfate activity in the solution. The fact that this termination is distinctively more stable than the alternatives is compatible with the experimental finding that PA (111) surfaces grow via screw-dislocations building large flat terraces. With the proposed surface structure we can also explain the experimental finding of different agglomerative bond strengths between different combinations of PA faces. This theoretical investigation could not clearly determine whether reconstruction or the enrichment of counterions above a charged and un-reconstructed surface plays the major role in stabilizing the PA (111) surface. However, we did find that in a simulation of the systems at atomic scale resolution with a reasonable model potential, a charged surface can appear as stable as the corresponding reconstructed one. As long as there is no experimental evidence to prove the opposite we must assume the chg-AlS-t model to represent a valid model of the PA (111) surface in solution. This is a nontrivial finding, with implications beyond the PA case, because the existence of such an un-reconstructed termination of a polar ionic crystal surface is usually excluded a priori.

Acknowledgment. The EPSRC are thanked for support under the Chemists and Chemical Engineers program grant GR/M73156/01.

References and Notes

(1) Sinfelt, J. H. *Surf. Sci.* **2002**, *500*, 923−946.
(2) Vlieg, E. *Surf. Sci.* **2002**, *500*, 458−474.
(3) Haberlein, H.; Tschiersch, K. P. *Pharmazie* **1994**, *49*, 769−775.
(4) Talapin, D. V.; Poznyak, S. K.; Gaponik, N. P.; Rogach, A. L.; Eychmuller, A. *Physica E* **2002**, *14*, 237−241.
(5) Pratola, F.; Simons, S. J. R.; Jones, A. G. *Chem. Eng. Res. Des.* **2002**, *80*, 441−448.
(6) Nygren, M. A.; Pettersson, L. G. M.; Freitag, A.; Staemmler, V.; Gay, D. H.; Rohl, A. L. *J. Phys. Chem.* **1996**, *100*, 294−298.
(7) Oliver, P. M.; Parker, S. C.; Egdell, R. G.; Jones, F. H. *J. Chem. Soc., Faraday Trans.* **1996**, *92*, 2049−2056.
(8) Baudin, M.; Wojcik, M.; Hermansson, K. *Surf. Sci.* **1997**, *375*, 374−384.
(9) Kotomin, E. A.; Heifets, E.; Maier, J.; Goddard, W. A. *Phys. Chem. Chem. Phys.* **2003**, *5*, 4180−4184.
(10) Safran, S. A. *Statistical Thermodynamics of Surfaces, Interfaces, and Membranes*; Addison-Wesley Publishers: Reading, MA, 1994.
(11) Allen, M.; Tildesley, D. *Computer Simulation of Liquids*; Clarendon Press: Oxford, U.K., 1987.
(12) Hodel, A.; Simonson, T.; Fox, R. O.; Brunger, A. T. *J. Phys. Chem.* **1993**, *97*, 3409−3417.
(13) Smith, P.; Lynden-Bell, R. M. *Mol. Phys.* **1999**, *96*, 1027−1032.
(14) Grochola, G.; Russo, S. P.; Snook, I. K.; Yarovsky, I. *J. Chem. Phys.* **2002**, *116*, 8547−8555.
(15) Broughton, J. Q.; Gilmer, G. H. *J. Chem. Phys.* **1986**, *84*, 5759−5768.
(16) Lill, J. V.; Broughton, J. Q. *Model. Simul. Mater. Sci. Eng.* **2000**, *8*, 345−355.
(17) Heifets, E.; Kotomin, E. A.; Maier, J. *Surf. Sci.* **2000**, *462*, 19−35.
(18) Watson, G. W.; Oliver, P. M.; Parker, S. C. *Phys. Chem. Miner.* **1997**, *25*, 70−78.
(19) Aquilano, D.; Rubbo, M.; Catti, M.; Pavese, A. *J. Cryst. Growth* **1997**, *182*, 168−184.
(20) Conesa, J. C. *Surf. Sci.* **1995**, *339*, 337−352.
(21) Gillan, M. J.; Kantorovich, L. N.; Lindan, P. J. D. *Curr. Opin. Solid State Mater. Sci.* **1996**, *1*, 820−826.
(22) Larson, A. C.; Cromer, D. T. *Acta Crystallogr.* **1967**, *A22*, 793−800.
(23) Berendsen, H. J. C.; Grigera, J. R.; Straatsma, T. P. *J. Phys. Chem.* **1987**, *91*, 6269−6271.
(24) Sakuntala, T.; Akhilesh, K. A.; Chandra Shekar, N. V.; Sahu, P. C. *J. Phys.: Condens. Matter* **2000**, *12*, 4417−4432.
(25) Amara, N.; Ratsimba, B.; Wilhelm, A. M.; Delmas, H. *Ultrason. Sonochem.* **2001**, *8*, 265−270.
(26) Vanenckevort, W. J. P.; Bennema, P.; Vanderlinden, W. H. *Z. f. Phys. Chem. Wiesbaden* **1981**, *124*, 171−191.
(27) Reyhani, M. M.; Freij, S.; Parkinson, G. M. *J. Cryst. Growth* **1999**, *198−199*, 258−263.
(28) Tasker, P. W. *J. Phys. C: Solid State Phys.* **1979**, *12*, 4977−4984.
(29) Smith, W.; Forester, T. R. *J. Mol. Graph.* **1996**, *14*, 136−141.
(30) Essmann, U.; Perera, L.; Berkowitz, M. L.; Darden, T.; Lee, H.; Pedersen, L. G. *J. Chem. Phys.* **1995**, *103*, 8577−8593.
(31) Yeh, I. C.; Berkowitz, M. L. *J. Chem. Phys.* **1999**, *111*, 3155−3162.
(32) Bogusz, S.; Cheatham, T. E.; Brooks, B. R. *J. Chem. Phys.* **1998**, *108*, 7070−7084.
(33) Hoover, W. G. *Phys. Rev.* **1985**, *A31*, 1695−1697.
(34) Smith, W.; Fincham, D. *Mol. Simul.* **1993**, *10*, 67−71.
(35) Gale, J. D. *J. Chem. Soc., Faraday Trans.* **1997**, *93*, 629−637.
(36) Allan, N. L.; Rohl, A. L.; Gay, D. H.; Catlow, C. R. A.; Davey, R. J.; Mackrodt, W. C. *Faraday Discuss.* **1993**, *95*, 273−280.
(37) Borodin, O.; Bell, R. L.; Li, Y.; Bedrov, D.; Smith, G. D. *Chem. Phys. Lett.* **2001**, *336*, 292−302.
(38) Rudolph, W. W.; Mason, R.; Pye, C. C. *Phys. Chem. Chem. Phys.* **2000**, *2*, 5030−5040.
(39) Adamson, A. W.; Gast, A. P. *Physical Chemistry of Surfaces*; John Wiley & Sons: New York, 1997.
(40) Chang, T. M.; Dang, L. X. *J. Phys. Chem. B* **1999**, *103*, 4714−4720.
(41) Liu, D.; Lu, H. M.; Hardy, J. R.; Ullman, F. G. *Phys. Rev.* **1991**, *B44*, 7387−7393.
(42) Kato, E.; Daimon, K. *J. Ceram. Soc. Jpn.* **1979**, *87*, 590−595.
(43) Manoli, J. M.; Herpin, P.; Pannetier, G. *Bull. Soc. Chim. Fr.* **1970**, *1970*, 98−101.
(44) Haussuehl, S. *Z. Kristallogr.* **1961**, *116*, 371−405.
(45) Marcus, Y. *Chem. Rev.* **1988**, *88*, 1475.
(46) Bol, W.; Welzen, T. *Chem. Phys. Lett.* **1977**, *49*, 189.
(47) Caminiti, R.; Paschina., G.; Pinna., G. *Chem. Phys. Lett.* **1979**, *64*, 391−395.
(48) Ohtaki, H.; Radnai, T. *Chem. Rev.* **1993**, *93*, 1157.
(49) McCall, D. W.; Douglas, D. C. *J. Phys. Chem.* **1965**, *69*, 2001.